Title

High Ammonia Adsorption in MFM-300 Materials: Dynamics and Charge Transfer in Host—Guest Binding

Journal

Journal of the American Chemical Society, 143(8)

ISSN

0002-7863

Authors

Han, Xue

Lu, Wanpeng

Chen, Yinlin

et al.

Publication Date

2021-03-03

DOI

10.1021/jacs.0c11930

Peer reviewed

High ammonia adsorption in MFM-300 materials: dynamics and charge-transfer in host-guest binding

Xue Han,[1†] Wanpeng Lu,[1†] Yinlin Chen,[1] Ivan da Silva,[2] Jiangnan Li,[1] Longfei Lin,[1] Weiyao Li,[1] Alena M. Sheveleva,[1,3] Harry G. W. Godfrey,[1] Zhenzhong Lu,[1] Floriana Tuna,[1,3] Eric J. L. McInnes,[1,3] Yongqiang Cheng,[4] Luke L. Daemen,[4] Laura J. M^{c}Cormick M^{c}Pherson[5], Simon J. Teat[5], Mark D. Frogley[6], Svemir Rudic,[2] Pascal Manuel,[2] Anibal J. Ramirez-Cuesta,[4] Sihai Yang[1]* and Martin Schröder[1]*

1. Department of Chemistry, University of Manchester, Manchester, M13 9PL, UK
2. ISIS Facility, Science and Technology Facilities Council (STFC), Rutherford Appleton Laboratory, Didcot, OX11 0QX, UK
3. Photon Science Institute, University of Manchester, Manchester, M13 9PL, UK
4. Neutron Scattering Division, Neutron Sciences Directorate, Oak Ridge National Laboratory, Oak Ridge, TN 37831, USA
5. Advanced Light Source, Lawrence Berkeley National Laboratory, Berkeley, CA 94720 (USA)
6. Diamond Light Source, Harwell Science Campus, Oxfordshire, OX11 0DE (UK)

[†]*: Authors contributed equally to this work.*

ABSTRACT: NH_3 (ammonia) is a promising energy resource owing to its high hydrogen density. However, its widespread application is restricted by the lack of efficient and corrosion-resistant storage materials. Here, we report high NH_3 adsorption in a series of robust metal-organic framework (MOF) materials, MFM-300(M) (M = Fe, V, Cr, In). MFM-300(M) (M = Fe, V^{III}, Cr) show fully reversible capacity for >20 cycles, reaching capacities of 16.1, 15.6 and 14.0 mmol g^{-1}, respectively, at 273 K and 1 bar. Under the same condition, MFM-300(V^{IV}) exhibits the highest uptake among this series of MOFs of 17.3 mmol g^{-1}. *In situ* neutron powder diffraction, single crystal X-ray diffraction and electron paramagnetic resonance spectroscopy confirm that the redox-active V centre enables host-guest charge-transfer, with V^{IV} being reduced to V^{III} and NH_3 oxidised to hydrazine, N_2H_4. A combination of *in situ* inelastic neutron scattering and DFT modelling has revealed the binding dynamics of adsorbed NH_3 within these MOFs to afford a comprehensive insight into the application of MOF materials to the adsorption and conversion of NH_3.

Nearly 200 million tons of NH_3 (ammonia) are produced annually across the world. NH_3 is widely considered as one of the most viable media for hydrogen storage and distribution due to its high volumetric (~0.105 kg/L or 3.6 kWh/L at 25 °C) and gravimetric (17.7 wt.% or 5.8 kWh/kg) hydrogen energy densities [1]. It is also recognized as a renewable fuel which can be produced at scale, at low cost and combusted in fuel cells to yield H_2O and N_2 as products[2]. These favourable properties make NH_3 a promising potential hydrogen carrier for on-board storage. However, several prerequisites need to be fulfilled for any practical application, including the development of safe and high-capacity storage media, efficient cracking processes, and an effective system for capture and removal of NH_3 that may leak. Even 0.1 ppm NH_3 can poison the proton exchange membranes within fuel cells [3].

A variety of conventional sorbent materials have been investigated for NH_3 capture and storage, but these tend to show limited capacities. Examples include resins (11.4 mmol g^{-1} in Amberlyst 15 [4]), zeolites (9.3 mmol g^{-1} in 13X zeolite [5]) and mesoporous silica (8.8 mmol g^{-1} in MCM-41[6]). The presence of surface acidic functionalities [7], especially hydroxyl, carboxyl groups, and open metal sites [8] can significantly enhance NH_3 uptake. Therefore, hybrid MOF materials with high porosity and accessible functional groups have attracted increasing attention for NH_3 adsorption[9]. For example, $[Cu_2Cl_2(BBTA)]$ [H_2BBTA= 1*H*,5*H*-benzo(1,2-*d*:4,5-*d*')bistriazole] incorporating open metal sites shows an exceptional NH_3 uptake of 19.8 mmol g^{-1} at 298 K and 1 bar[10]. $[M_2Cl_2(BTDD)]$ (H_2BTDD = bis(1*H*-1,2,3-triazolo[4,5-*b*],[4',5'-*i*])dibenzo[1,4]dioxin; M = Mn, Co, Ni) with extended linkers also exhibited high and reversible NH_3 uptakes of 15.47, 12.00, and 12.02 mmol/g, respectively, for up to 3 cycles[11]. DUT-6 functionalised with aromatic hydroxyl groups also exhibits a high NH_3 uptake of 16.4 mmol/g at 298 K and 1 bar[12]. However, as with DUT-6 and many

other systems, structural degradation occurs over time due to the highly corrosive nature of NH_3, especially at high concentrations, and this often leads to irreversible adsorption [13]. To date, stable MOFs showing reversible and high NH_3 adsorption remain rare. Additionally, the binding dynamics of adsorbed NH_3 molecules within MOFs have not been reported to date owing in part to the complexity of the molecular modes of NH_3, even at cryogenic temperatures.

The highly stable MOF, MFM-300(Al), exhibits fully reversible adsorption of NH_3 (15.7 mmol g^{-1} at 273 K and 1 bar), and more intriguingly, the packing density of NH_3 within the pores approaches that of liquid NH_3 [14]. The stable isostructural analogues MFM-300(M) (M = Fe, Cr, In) can be prepared, in addition to the the redox-active MFM-300(M) (M = V^{III}, V^{IV})[15]. The rigid scaffold of these MFM-300 materials provides an excellent platform to interrogate the dynamics of adsorbed NH_3 molecules. We report the systematic study of NH_3 adsorption in these MOFs by both isotherm and dynamic breakthrough experiments. The preferred binding domains of NH_3 guest molecules have been determined by *in situ* synchrotron X-ray single crystal diffraction and neutron powder diffraction (NPD). We also report the first investigation of the dynamics of adsorbed NH_3 molecules within MOFs by *in situ* inelastic neutron scattering (INS) to understand the host-guest binding interactions. MFM-300(V^{IV}) was of particular interest since it not only shows the highest NH_3 uptake, but also it undergoes a host-guest charge-transfer leading to the oxidation of adsorbed NH_3 to hydrazine (N_2H_4) within the pore.

Results and Discussion

Analysis of NH_3 adsorption isotherms and breakthrough curves

The NH_3 adsorption isotherms from 0-1.0 bar between 273 and 323 K were measured for the MFM-300 series under investigation (Figure 1 a-d). The NH_3 uptakes at 273 K and 1.0 bar were measured as 14.0, 16.1, 15.6 and 17.3 mmol g^{-1} for MFM-300(M) (M = Cr, Fe, V^{III}, V^{IV}), respectively. These uptake values compare favourably with the leading sorbent materials for NH_3 in literature (Table S13), and all of the MFM materials show high framework stability and an increase of isothermal uptakes with decreasing temperature (Figure 1). The isosteric heats of adsorption (Q_{st}) calculated from these isotherms at different temperatures are in the range of 30-65 kJ mol^{-1} (Table 1). Notably though, MFM-300(In) shows significant loss of NH_3 capacity over repeated cycles (Figure S1), and is unstable under these conditions.

MFM-300(M) (M = Cr, Fe, V^{III}) all display reversible uptake of NH_3 with consistent adsorption capacities over 20 cycles of adsorption/desorption of NH_3 under pressure-swing conditions. The residual amount of NH_3 left in MFM-300(M) (M = Cr, Fe, V^{III}) on degassing is ~9% , but this can be readily desorbed by heating at 333 K for 2 h (Figure 1e-h). In contrast, MFM-300 (V^{IV}) shows a hysteresis loop, characteristic of capillary condensation in mesopores and/or due to a broad distribution of pore size and shape[16] (Figure 1a-d). Considering the pore size (~6.7 x 6.7 $Å^2$) of MFM-300(V^{IV}), this result suggests a specific and potentially strong host-guest binding upon the adsorption of NH_3 in this material. MFM-300(V^{IV}) also exhibits an intriguing *increase* of both capacity and residue within the first 18 cycles. The residual amount of NH_3 left within MFM-300(V^{IV}) upon regeneration by pressure-swing steadily increases from 8 to 20% along these cycles indicating an accumulation of strongly-bound NH_3-derived species in MFM-300(V^{IV}), which cannot be desorbed by reducing pressure alone. This residue can be removed by heating under dynamic vacuum, but some structural degradation of the MOF also occurs. Interestingly, the regenerable component of the NH_3 sorption capacity of MFM-300(V^{IV}) remains unchanged over cycles, indicating that the accumulated residue derived from NH_3 does not adversely affect the sorbent capacity; the structural integrity of MFM-300(V^{IV}) after these cycles is confirmed by powder X-ray diffraction (PXRD) (Figure 1i).

The ability of these MOFs to capture NH_3 at low concentration (1000 ppm) was confirmed by dynamic breakthrough experiments (Figure 1j) at 298 K. The dynamic NH_3 uptake calculated from these breakthrough curves are 1.1, 0.6, 1.9 and 1.0 mmol g^{-1} for MFM-300(M) (M = Cr, Fe, V^{III}, and V^{IV}), respectively. While MFM-300(V^{IV}) exhibits the highest isothermal uptake, MFM-300(V^{III}) demonstrates the maximum retention of NH_3 under dynamic conditions. The discrepancy between isothermal and dynamic uptake is widely acknowledged,[17] as the nature of these two types of experiments is fundamentally different. Breakthrough experiments are undertaken at the ppm level of NH_3 under flow conditions, whereas isotherms were measured statically with pure NH_3. Kinetic and thermodynamic factors therefore need to be taken into account in such experiments.

Determination of preferred binding domains of ND_3

Neutron powder diffraction (NPD) data for ND_3-loaded MFM-300 were collected at 10 K (ratio of ND_3: M = 0.3, 0.5, 2.2, 2.2 for M = In, V^{III}, Fe, V^{IV}, respectively). Notwithstanding its low stability to NH_3, NPD confirmed that MFM-300(In) retains its structure at low loadings of ND_3, and Rietveld refinement of these data illustrated distinct binding sites for ND_3 (Figure 2). Two binding sites for ND_3 are found in MFM-300(M) (M = In, V^{III}) and an additional site for ND_3 was located in MFM-

300(Fe) due to the higher ND_3 loading in this latter experiment. Site I has the highest occupancy with hydrogen bonding between the O_{bridge}-H···ND_3 (1.411-1.978 Å) involving the bridging hydroxyl groups of the MOF. This is supplemented by further hydrogen bonding ($H_{aromatic}$···ND_3 = 2.738-3.174 Å; ND_3···O_{ligand} =3 .078-3.179 Å) and electrostatic interactions (ND_3···aromatic rings = 2.946-3.132 Å).

Hydrogen/deuterium site exchange is also observed between the adsorbed ND_3 and the H-O_{bridge} group on the framework MFM-300(M) (M = In, Fe, V^{III}), which is similar to that observed in ND_3-loaded MFM-300(Al)[14]. Site II is located further towards the centre of the pore and is anchored in place through hydrogen bonding interactions (ND_3···O_{ligand} = 2.284-3.065 Å). Site III in MFM-300(Fe) is primarily stabilised by electrostatic interactions (ND_3··· aromatic rings = 3.146 Å). In MFM-300(Fe), intermolecular hydrogen bonds between ND_3 molecules (2.327-3.193 Å) were also observed, and these propagate along the 1D channel to form a cooperative $\{ND_3\}_\infty$ network. These multiple interactions between molecules of ND_3 are similar to those observed in solid ND_3 at 2 K (N···D = 2.357 Å) [18].

MFM-300(V^{IV}) does not incorporate bridging hydroxyl groups but rather has bridging oxo centres to balance the charge of the oxidised V centre.[15] Thus, hydrogen bonding to hydroxyl groups as above is not possible and the guest molecules are located towards the centre of the pore. Interestingly, unlike MFM-300(M) (M = In, Fe, V^{III}), where adsorbed ND_3 molecules remain chemically intact in the pore, in MFM-300(V^{IV}) a molecule of N_2D_4 molecule is identified at site II with an ND_3 molecule at site I being partially protonated to ND_4^+. The bridging oxo centres remain unprotonated. Both sites are stabilised through hydrogen bonding (ND_3···O_{ligand} = 2.529-3.092 Å) and the amount of N_2D_4 at site II is calculated to be 0.5 N_2H_4 per V centre, consistent with the redox equilibrium based upon a complete reduction of V^{IV} to V^{III} centres.

Studies of host-guest charge transfer

The oxidation state of the V centers in MFM-300(V^{IV}) before and after NH_3 adsorption was investigated by X-band (9.86 GHz) electron paramagnetic resonance (EPR) at room temperature (Figure 3a). In six-coordinate O_h symmetry, the d^2 V^{III} centre has a triplet ground state ($^3T_{1g}$). Lower symmetry removes orbital degeneracy resulting in a singlet ground state with S = 1, where spin-orbit coupling leads to a large zero-field splitting (up to tens of cm^{-1}). Therefore, most V^{III} species are EPR-silent at X-band frequencies, which is also the case for MFM-300(V^{III}). Bare MFM-300(V^{IV}) however shows a single resonance centred at g = 1.955, consistent with a d^1 V^{IV} centre, and a broad peak-to-peak linewidth is measured at *ca.* 130 G due to the exchange interactions in the V^{IV} centre. Upon loading of NH_3, this signal decreases significantly, suggesting the reduction of V^{IV} to V^{III} centres in MFM-300(V^{IV}). Thus, the redox activity of MFM-300(V^{IV}) promotes a host-guest charge-transfer between the MOF and the adsorbed ND_3 molecules, resulting in the reduction of V^{IV} centers and concomitant oxidation of NH_3 to N_2H_4. Interestingly, the N_2H_4 molecules can be removed from the pores by soaking the NH_3-saturated MFM-300(V) in water as confirmed by the Watt and Chrisp method[19], where a characteristic UV-vis absorption band at 460 nm was observed for the filtrate (see SI).

To gain further insights into the host-guest charge-transfer in MFM-300(V), we sought to monitor directly the change of oxidation state of V centres by bond valence sum (BVS) calculations. Because V is almost transparent in neutron diffraction, a series of *in situ* synchrotron X-ray single-crystal diffraction experiments of MFM-300(M) (M = V^{III}, V^{IV}) were collected at different NH_3 loadings (Figure 4). As expected, little change in the oxidation state of the V centre (3.05-3.10) was observed for MFM-300(V^{III}) upon loading with NH_3 (Table S6, Figure S10-S14). Bare MFM-300(V^{IV}) exhibits an oxidation state of 3.70 for the V centre, and no substantial change was observed at low NH_3 loadings (3.70, 3.67 and 3.62 for $VC_8O_5H_3{\cdot}0.2NH_3$, $VC_8O_5H_3{\cdot}1.1NH_3$ and $VC_8O_5H_3{\cdot}2.5NH_3$, respectively, Table S7), consistent with the absence of N_2H_4 molecules in the pore. However, when the loading is increased to $VC_8O_5H_3{\cdot}3.9NH_3$, the oxidation state of the V centre exhibits an apparent drop to 3.52, and simultaneously a molecule of N_2H_4 is observed as the occupancy of N at site III (H is invisible) exceeded 0.5 [N···N = 1.61(9) Å, 1.56(14) Å]. These results suggest that the charge-transfer between adsorbed NH_3 molecules and the V^{IV} centre can only occur when the loading of NH_3 is sufficiently high so that a predominant occupancy of the N site, which is located close to the metal chain, is reached to initiate the redox reaction. Interestingly, this N site {site I in dataset $VC_8O_5H_3{\cdot}0.3NH_3$-*regenerate* (Figure S21)} is preserved after the sample was degassed under dynamic vacuum at 298 K for 2 h, corresponding to a residual of approximately 7.5% of the adsorption capacity. This is in excellent agreement with that (~8%) observed in the pressure-swing experiment.

Analysis of host-guest binding dynamics

Combined INS and DFT have been employed to interpret the dynamics of adsorbed NH_3 molecules within MFM-300(M) (M = Al, Fe, V^{III}, V^{IV}). Vibrational features of both the NH_3 guests and the framework host were successfully captured and assigned based upon DFT calculations using the structural models derived from NPD analyses.

Excellent agreement between experimental and simulated INS spectra were observed for MFM-300(M) (M = Al, Fe, V^{III}) (Figure 5). MFM-300(V^{IV}) exhibits broad INS features that show discrepancies compared with the simulated INS spectra because of the complex and disordered arrangement of NH_3, NH_4^+ and N_2H_4 within the pore, and these had to be simplified within the DFT calculations, which cannot consider the presence of hopping of H centers between sites. This, however, is consistent with the reactive adsorption of NH_3 and the host-guest charge-transfer process that takes place in MFM-300(V^{IV}) with NH_3. Distinct peaks are observed in the INS difference spectra obtained by subtracting the features of the bare MOF and sample cell from the spectra of NH_3-loaded MOF. Peaks in the low energy region (below 60 meV) are primarily due to the vibrational modes of adsorbed NH_3 molecules, with a small contribution due to changes in the lattice modes of the framework. The features in the higher energy region (80-200 meV) mainly reflect the modes of the framework.

At a loading of $1NH_3$ per Al centre in NH_3@MFM-300(Al), peak I at 6.2 meV represents the translational motion of NH_3 along directions perpendicular to the N···H-$O_{bridging}$ bond, whereas peak II at 13.8 meV is due to the translational motion along the direction of the N···H-$O_{bridging}$ bond (Figure 5a, b). Peaks III-V (16.1, 19.8, 22.3 meV, respectively) are due to the librational (torsional) motion of NH_3 around its C_3 axis, as well as translational-torsional hybrid motions. Peaks VI-VII at higher energy (34.0, 40.1 meV, respectively) originate from the rocking motions of NH_3 around the N center. When comparing this spectrum to that of the solid NH_3 (transitional modes: 8.7-21.0 meV; librational modes: 29.4-32.3 meV; rocking modes: 39.3-54.4 meV), a red-shift of all peaks in the three regions was observed for the adsorbed NH_3 molecules. This reflects the local environment of the adsorbed NH_3 which interacts to the hydroxyl group in the framework via hydrogen bonding, in contrast to the extensive 3D hydrogen bonding network formed between 6 adjacent NH_3 molecules in its solid-state structure. The former affords greater flexibility to the adsorbed NH_3 molecules, whereas the latter imposes more restrictions to intermolecular motions. Another observation is that the INS peaks for the adsorbed NH_3 molecules are broader than those in the pure solid phase, most notably for the transitional and librational region. This can be attributed to the isolated environment for the adsorbed molecules causing uncorrelated vibrations of individual NH_3. In contrast, in crystalline NH_3 the molecules are strongly restrained and vibrate in phase, giving sharp and distinct peaks on the INS spectrum.

INS peaks observed MFM-300(Al) at (i) 87.6, (ii) 114, (iii) 118 and (iv) 143 meV can be assigned to H-C out-of-C_6 plane deformation (in phase along ring, meaning H atoms move in the same direction), H-C out-of-C_6 plane deformation (anti-phase along ring, meaning neighbouring H atoms move in opposite directions), H-O in V-O-V-plane bending and H-C in-C_6-plane bending modes, respectively (Figure 5c, e). Upon adsorption of NH_3 into the framework, peak (i) shifts slightly to higher energy, indicating a stiffening effect of the phenyl rings due to the interaction with NH_3, whereas peak (iv) retains its position and exhibits an intensity change only, suggesting these modes are weakly affected by the NH_3 molecules. The effect of NH_3 upon peak (ii) is phase-dependent, where the mode that involves more displacement of β-H is affected more strongly due to the shorter distance between the NH_3 to β-H than that of the α-H. Overall, the INS analysis is in excellent agreement with the crystal structures determined from NPD experiments and demonstrates that the adsorbed NH_3 molecules interact primarily with the H centers of hydroxyl groups and the C_6 ring at the β position. Detailed spectral interpretations of MFM-300(M) (M = Fe, V^{III}, V^{IV}) on loading with NH_3 loading are discussed in the SI (Figure S22-S24, Table S10-S12).

Single crystals of MFM-300(M) (M = Fe, V^{III}, V^{IV}) have been examined further by *in situ* synchrotron FTIR micro-spectroscopy at various NH_3 partial pressures in a flow cell. MFM-300(V^{III}) shows that the characteristic O-H stretching mode of the bridging hydroxyl group at 3642 cm^{-1}, and the N-H stretching mode (3300-3400 cm^{-1}) of adsorbed NH_3 molecules increase steadily with increasing NH_3 loading (Figure 3b). In contrast, bare MFM-300(V^{IV}) displays no adsorption bands above 3600 cm^{-1} due to the absence of the bridging hydroxyl moiety (Figure 3c). The N-H stretching mode of NH_3 at 3374 cm^{-1} grows with the increase of NH_3 partial pressure. Simultaneously, FTIR bands at 970 cm^{-1}, 3160 cm^{-1} and 3210 cm^{-1}, assigned to -NH_2 rocking, -NH_2 symmetrical stretching, and -NH_2 anti-symmetrical stretching of N_2H_4, respectively,[20] are observed with increasing absorbance as the loading of NH_3 increases. Moreover, these bands assigned to N_2H_4 remain on treating the material under dynamic vacuum at room temperature, consistent with the residual uptake that was observed in the adsorption and crystallographic experiments.

Conclusions

Powerful drivers exist for the development of functional materials for NH_3 storage. This work presents a comprehensive study of NH_3 adsorption in porous MFM-300 sorbents. MFM-300(M) (M = Al, Cr, Fe, V^{III}, V^{IV}) show excellent reversible uptake capacity for NH_3 coupled with high framework stability with great potential for NH_3 capture and storage. Interestingly, the redox-active MFM-300(V^{IV}) drives the oxidation of adsorbed NH_3 to N_2H_4, which is accompanied by reduction of V^{IV} to V^{III}, and promotes the NH_3

adsorption uptake up to 17.3 mmol g^{-1}. Combined INS and DFT studies have afforded an in-depth analysis of the binding dynamics of NH_3 in these materials. This study will inspire the future development of porous materials with an integrated function for the storage, capture and conversion for NH_3.

ASSOCIATED CONTENT

Supporting Information. Supporting Information includes additional experimental details, adsorption isotherm and uptake data, powder X-ray and neutron diffraction data, views of crystal structures, CIF files, EPR and FTIR spectroscopy, INS data, and details for detection of N_2H_4. This material is available free of charge via the Internet at http://pubs.acs.org.

AUTHOR INFORMATION

Corresponding Author

*Sihai.Yang@manchester.ac.uk
*M.Schroder@manchester.ac.uk

Author Contributions

†X. Han and W. Lu contributed equally.

Notes

The authors declare no competing financial interests.

ACKNOWLEDGMENT

We thank EPSRC (EP/I011870), the Royal Society and University of Manchester. This project has received funding from the European Research Council (ERC) under the European Union's Horizon 2020 research and innovation programme (grant agreement No 742401, NANOCHEM). We are grateful to Diamond Light Source and STFC/ISIS Facility for access to Beamlines B22 and TOSCA/WISH, respectively, and to Oak Ridge National Laboratory for access to the VISION spectrometer at the Spallation Neutron Source. This research used resources of Beamlines 11.3.1 and 12.2.1 at the Advanced Light Source, which is a DOE Office of Science User Facility under contract no. DE-AC02-05CH11231. The computing resources were made available through the VirtuES and the ICE-MAN projects, funded by Laboratory Directed Research and Development program and Compute and Data Environment for Science (CADES) at ORNL. JL thanks China Scholarship Council (CSC) for funding. AMS is supported by a Royal Society Newton Fellowship.

REFERENCES

[1] Dong, B. X.; Tian, H.; Wu, Y. C.; Bu, F. Y.; Liu, W. L.; Teng, Y. L.; Diao, G. W. Improved electrolysis of liquid ammonia for hydrogen generation via ammonium salt electrolyte and Pt/Rh/Ir electrocatalysts. *Int. J. Hydrog. Energy*. **2016**, *41*, 14507-14518.

[2] MacFarlane, D. R.; Cherepanov, P. V.; Choi, J.; Suryanto, B. H.; Hodgetts, R. Y.; Bakker, J. M.; Ferrero Vallana, F. M.; Simonov, A. N. A roadmap to the ammonia economy. *Joule*. **2020**, *4*, 1186-1205.

[3] Uribe, F.; Brosha, E.; Garzon, F.; Mikkola, M.; Pivovar, B.; Rockward, T.; Valerio, J.; Wilson, M. VII. I. 4 Effect of fuel and air impurities on PEM fuel cell performance. *Hydrog. energy. gov*. **2005**, 1046-1051.

[4] Helminen, J.; Helenius, J.; Paatero, E.; Turunen, I. Adsorption equilibria of ammonia gas on inorganic and organic sorbents at 298.15 K. *J. Chem. Eng*. **2001**, *46*, 391-399.

[5] Helminen, J.; Helenius, J.; Paatero, E.; Turunen, I. Comparison of sorbents and isotherm models for NH_3-gas separation by adsorption. *AIChE J*. **2000**, *46*, 1541-1555.

[6] Furtado, A. M.; Wang, Y.; Glover, T. G.; LeVan, M. D. MCM-41 impregnated with active metal sites: synthesis, characterization, and ammonia adsorption. *Micropor Mesopor Mat*. **2011**, *142*, 730-739.

[7] Mochizuki, T.; Kubota, M.; Matsuda, H.; Camacho, L. F. E. Adsorption behaviors of ammonia and hydrogen sulfide on activated carbon prepared from petroleum coke by KOH chemical activation. *Fuel Process. Technol*. **2016**, *144*, 164-169.

[8] Yang, Y.; Faheem, M.; Wang, L.; Meng, Q.; Sha, H.; Yang, N.; Yuan, Y.; Zhu, G. Surface pore engineering of covalent organic frameworks for ammonia capture through synergistic multivariate and open metal site Approaches. *Cent. Sci*. **2018**, *4*, 748-754.

[9] (a) Vikrant, K.; Kumar, V.; Kim, K. H.; Kukkar, D. Metal-organic frameworks (MOFs): potential and challenges for capture and abatement of ammonia. *J. Mater. Chem. A*. **2017**, *5*, 22877-22896. (b) Kim, K. C.; Yu, D.; Snurr, R. Q. Computational screening of functional groups for ammonia capture in metal-organic frameworks. *Langmuir*. **2013**, *29*, 1446-1456. (c) Chen, Y.; Zhang, X.; Ma, K.; Chen, Z.; Wang, X.; Knapp, J.; Alayoglu, S.; Wang, F.; Xia, Q.; Li, Z.; Islamoglu, T.; Farha, O. K. A zirconium-based metal-organic framework with 9-connected nodes for ammonia capture. *ACS Appl. Nano Mater*. **2019**, *2*, 6098-6102.

[10] Rieth, A. J.; Dincă, M. Controlled gas uptake in metal-organic frameworks with record ammonia sorption. *J. Am. Chem. Soc*. **2018**, *140*, 3461-3466.

[11] Rieth, A. J.; Tulchinsky, Y.; Dincă, M. High and reversible ammonia uptake in mesoporous azolate metal–organic frameworks with open Mn, Co, and Ni sites. *J. Am. Chem. Soc*. **2016**, *138*, 9401-9404.

[12] Spanopoulos,I.; Xydias, P.; Malliakas, C. D., Trikalitis, P.N. A straight forward route for the development of metal−organic frameworks functionalized with aromatic −OH groups: synthesis, characterization, and gas (N_2, Ar, H_2, CO_2, CH_4, NH_3) sorption properties. *Inorg. Chem.* **2013**, *52*, 855−862.

[13] (a) Katz, M. J.; Howarth, A. J.; Moghadam, P. Z.; DeCoste, J. B.; Snurr, R. Q.; Hupp, J. T.; Farha, O. K. High volumetric uptake of ammonia using Cu-MOF-74/Cu-CPO-27. *Dalton Trans*. **2016**, *45*, 4150-4153. (b) Shustova, N. B.; Cozzolino, A. F.; Reineke, S.; Baldo, M.; Dincă, M. Selective turn-on ammonia sensing enabled by high-temperature fluorescence in metal-organic frameworks with open metal sites. *J. Am. Chem. Soc*. **2013**, *135*, 13326-13329.

[14] Godfrey, H. G.; Da Silva, I.; Briggs, L.; Carter, J. H.; Morris, C. G.; Savage, M.; Dr. Timothy L. Easun; Manuel, P.; Murray. C. A.; Tang, C. C.; Frogley. M.; Cinque, G.; Yang, S.; Schröder, M. Ammonia storage by reversible host-guest site exchange in a robust metal-organic framework. *Angew. Chem. Int. Ed.* **2018**, *57*, 14778-14781.

[15] (a) Lu, Z.; Godfrey, H. G.; Da Silva, I.; Cheng, Y.; Savage, M.; Tuna, F.; McInnes, E. J. L.; Teat, S. J., Gagnon K. J.; Frogley, M. D.; Manuel, P.; Rudić, S.; Ramirez-Cuesta, A.J.; Easun, T. L.; Yang, S.; Schröder, M. Modulating supramolecular binding of carbon dioxide in

a redox-active porous metal-organic framework. *Nat. Commun*. **2017**, *8*, 1-10; (b) Han, X.; Hong, Y.; Ma, Y.; Lu, W.; Li, J.; Lin, L.; Sheveleva, A. M.; Tuna, F.; McInnes, E. J. L.; Dejoie, C.; Sun, J.; Yang, S.; Schröder, M. Adsorption of nitrogen dioxide in a redox active vanadium metal-organic framework material. *J. Am. Chem Soc*., **2020**, *142*, 15235-15239.

[16] Sing, K. S. Reporting physisorption data for gas/solid systems with special reference to the determination of surface area and porosity. *Pure Appl. Chem*. **1985**, *57*, 603-619.

[17] (a) Han, X.; Yang, S.; Schröder, M. Porous metal–organic frameworks as emerging sorbents for clean air. *Nat. Rev. Chem.* **2019**, 3, 108–118; (b) Sabouni., R.; Kazemian, H.; Rohani, S. Mathematical modeling and experimental breakthrough curves of carbon dioxide adsorption on metal organic framework CPM-5. *Environ. Sci. Technol.* **2013,** 47, 9372−9380; (c) Bozbiyik, B.; Assche; T. V.; Lannoeye, J.; De Vos, D. E.; Baron, G. V.; Denayer, J. F. M. Stepped water isotherm and breakthrough curves on aluminium fumarate metal–organic framework: experimental and modelling study. *Adsorption*. **2017**, 23, 185–192.

[18] Hewat, A. W.; Riekel, C. The crystal structure of deuteroammonia between 2 and 180 K by neutron powder profile refinement. *Acta Crystallogr. A*. **1979**, *35*, 569-571.

[19] Gamble, D. S.; Hoffman, I. Photometric analysis of trace amounts of hydrazine with p-dimethylaminobenzaldehyde. *Can. J. Chem*. **1967**, *45*, 2813-2819.

[20] Dirtu, D.; Odochian, L.; Pui, A.; Humelnicu, I. Thermal decomposition of ammonia. N_2H_4-an intermediate reaction product. *Open Chem. J*. **2006**, *4*, 666-673.

Figure 1. (a)-(d) Adsorption isotherms for NH_3 in MFM-300(M) (M = Cr, Fe, V^{III}, V^{IV}) at 273-328 K (adsorption: solid; desorption: open symbols). (e)-(h) Cyclic adsorption-desorption of NH3 in MFM-300(M) (M = (Cr, Fe, V^{III}, V^{IV}) at 298 K between 0-0.15 bar, dark-coloured bars show the residual NH3 left within the MOF after desorption under dynamic vacuum at 298 K. (i) PXRD patterns of as-synthesised MFM-300 and the samples after a cycle of adsorption and desorption of NH_3. (j) Breakthrough curves for NH_3 (1000 ppm diluted in He) through fixed beds packed with samples of MFM-300 samples at 298 K at 1.0 bar.

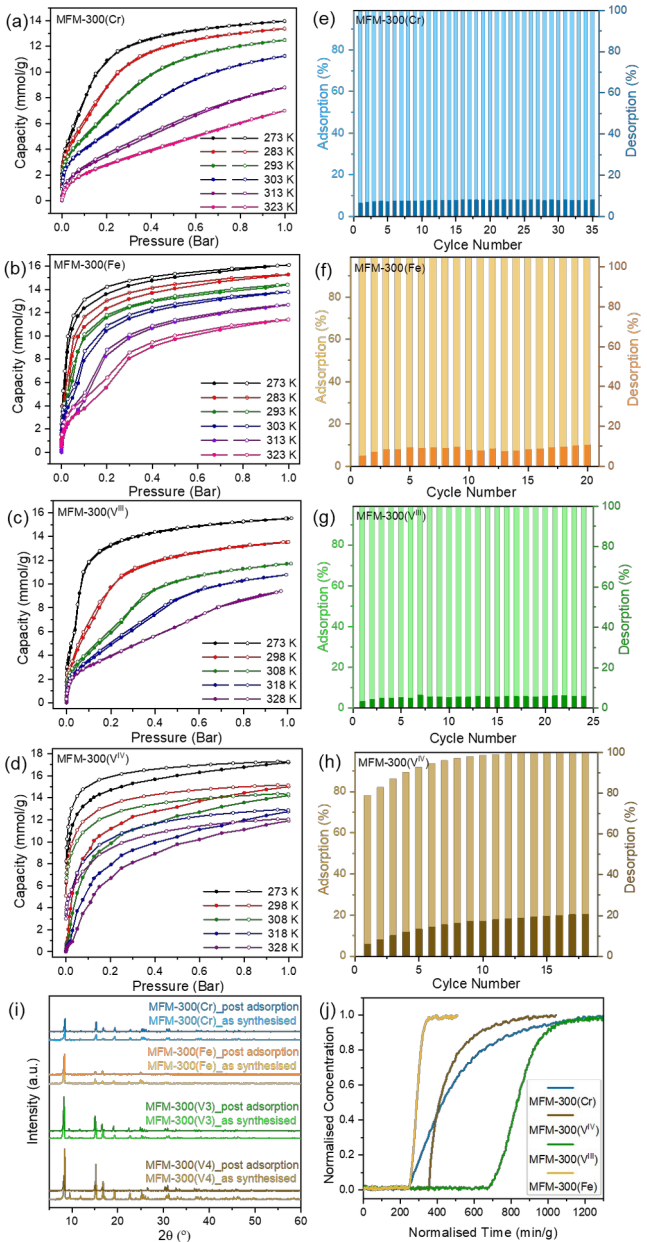

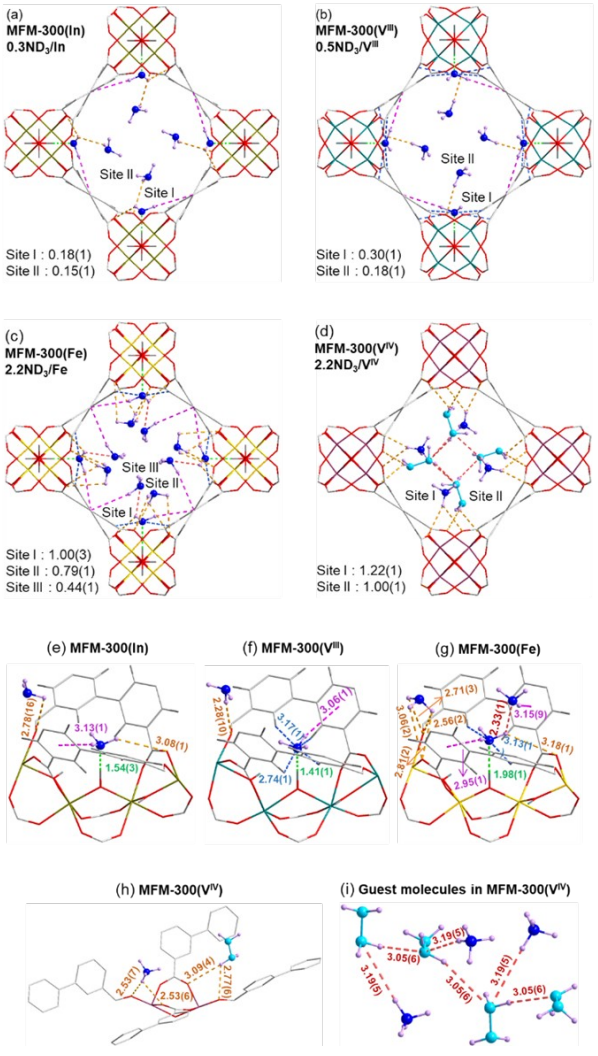

Figure 2. Views of sites for ND_3 in MFM-300(M) (M = In, V^{III}, Fe, V^{IV}) determined by neutron powder diffraction at 10 K. The occupancy of each site has been converted into ND_3/M for clarity. (a)-(d): Views along *c*-axis showing packing of the guest molecules within the pore. (e)-(h): Views of detailed host-guest interactions. (i): Cooperative network composed of N_2D_4 (N atoms: light blue) and ND_4^+ (N atoms: dark blue) in MFM-300(V). In: dark yellow; V^{III}: green; Fe: yellow; V^{IV}: magenta; O: red; C: white; H: grey; N: blue; D: purple.

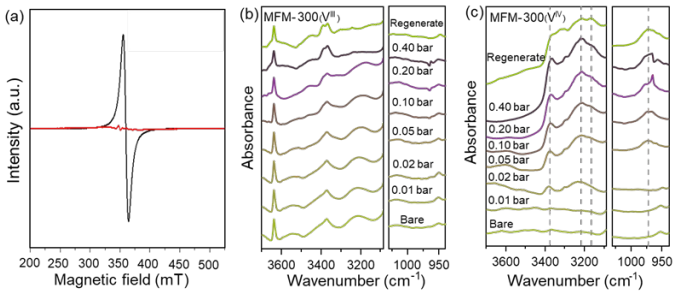

Figure 3. (a) X-band (9.87 GHz) EPR spectra of bare and NH_3-loaded MFM-300(V^{IV}). *In situ* synchrotron FTIR spectra for single-crystals of (b) MFM-300(V^{III}) and (c) MFM-300(V^{IV}) at various partial pressures of NH_3 (diluted in dry N_2) and after regeneration under a dry N_2 flow at 100 mL min^{-1} at 298 K for 2 hour.

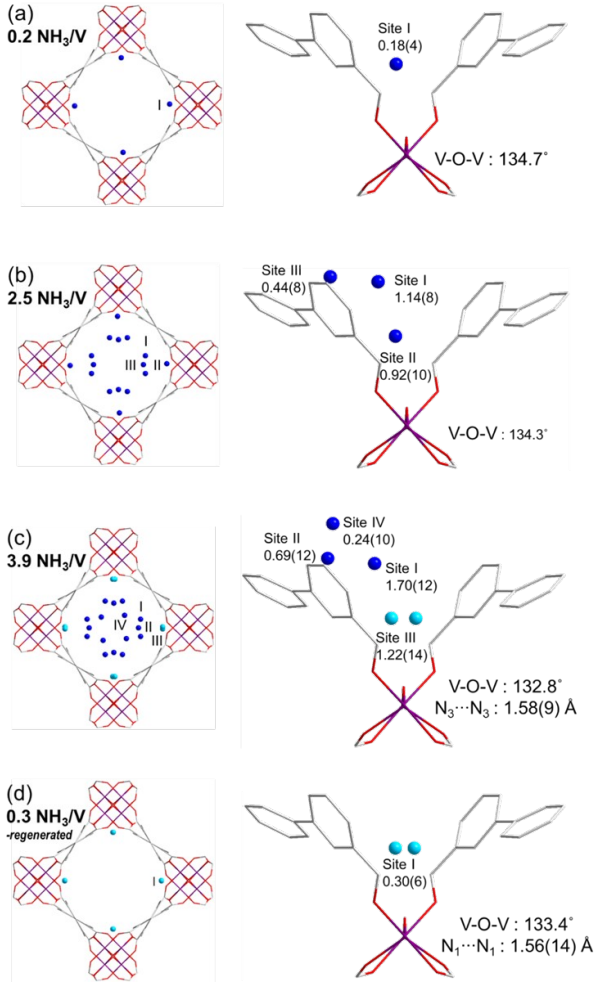

Figure 4. Views of single crystal X-ray structures of NH_3-loaded MFM-300(V^{IV}) along the *c*-axis (V: magenta; O: red; C: white; H: grey; N: light blue for N_2H_4, dark blue for NH_3 and NH_4^+). The structures were obtained from *in situ* synchrotron X-ray single crystal diffraction at 273 K, and the occupancy of

each site has been converted to NH_3/V^{IV} for clarity. (a)-(c) show the structure with increasing loading of NH_3 from 0.2 NH_3/V to 3.9 NH_3/V, and (d) shows the structure after the sample being degassed under dynamic vacuum at 298 K for 2h. N_2H_4 (N atoms: light blue) and NH_3 (N atoms: dark blue).

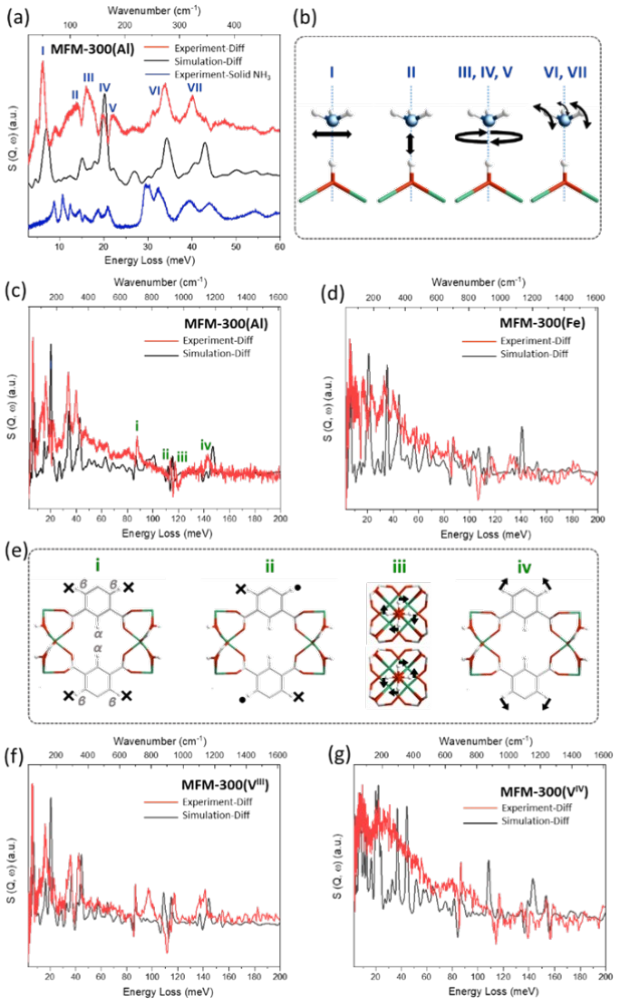

Figure 5. Comparisons of the experimental (red) and DFT-simulated (black) difference INS spectra of bare and NH_3-loaded MFM-300; (a) direct comparison with condensed NH_3 in the solid; (b), (e) vibrational modes of adsorbed NH_3 and of MFM-300(Al) host; (c),(d),(f),(g): difference INS spectra for NH_3 in MFM-300(M) (M = Al, Fe, V^{III}, V^{IV}), respectively.

Table 1. Summary of NH_3 adsorption in MFM-300 materials

MFM-300(M)	M = Al	M = V^{III}	M = V^{IV}	M = Cr	M= Fe
Uptake capacity[a] (mmol/g)	15.7	15.6	17.3	14.0	16.1
NH_3 Storage density in MOFs[a] (g/cm^3)	0.28	0.29	0.34	0.27	0.30
NH_3 Packing density in MOF pores[a] (g/cm^3)	0.72	0.54	0.61	0.51	0.60
NH_3 Packing density in MOF pores[b] (g/cm^3)	0.60	0.47	0.53	0.44	0.52
Pore Volume of MOF (cm^3/g)	0.37	0.49	0.48	0.47	0.46
Surface area (m^2/g)	1325	1755	1719	1683	1647
Enthalpy of adsorption (kJ/mol)	30 to 50	35 to 45	30 to 60	35 to 65	35 to 40
Entropy of adsorption [J/(mol·K)]	−240 to −135	−215 to −150	−240 to −180	−290 to −210	−215 to −175

[a]: at 273K 1 bar;

[b]: at 298K 1 bar.